

Principles of Surface-Directed Liquid Flow in Microfluidic Channels

Bin Zhao,[†] Jeffrey S. Moore,^{*,†} and David J. Beebe[‡]

The Beckman Institute for Advanced Science and Technology, University of Illinois at Urbana–Champaign, Urbana, Illinois 61801, and Department of Biomedical Engineering, The University of Wisconsin–Madison, Madison, Wisconsin 52706

To direct liquid flow inside microchannels, surface free energies were patterned by use of self-assembled monolayers (SAMs) in combination with either multistream laminar flow or photolithography. For the photolithographic method, two photocleavable SAMs were designed and synthesized. Carboxylic acid-terminated monolayers were obtained by photodeprotection, which was confirmed by contact angle and X-ray photoelectron spectroscopy. Using either of these patterning methods, we show that aqueous liquids flow only along the hydrophilic pathways when the pressure is maintained below a critical value; the liquids are referred to as being confined by virtual walls. Several principles of liquid flow in surface-patterned channels were derived analytically and verified experimentally. These principles include the maximum pressure that virtual walls can withstand, the critical width of the hydrophilic pathway that can support spontaneous flow, the smallest width of the liquid streams under an external pressure, the critical radius of curvature of turns that can be introduced into the hydrophilic pathway without liquid crossing the hydrophilic–hydrophobic boundary, and the minimal distance for two liquid streams to remain separated under the maximum pressure. Experimental results are in good agreement with the analytical predictions.

In recent years, tremendous efforts have been invested in miniaturizing and integrating chemical and physical processes such as mixing, separation, purification, and detection to create integrated microfluidic systems for chemical analysis and synthesis and bioassay.¹ The advantages of this so-called “lab-on-a-chip” technology lie in the consumption of a small amount of the sample and reagents, fast processing time, and high throughput compared to macroscopic systems. A critical issue in the design and fabrication of microfluidic devices is the manipulation of liquid and gaseous fluids within microchannel networks. Many techniques have been used to meter, transport, and position and mix liquid samples. These techniques include electroosmotic flow,²

mechanical pumping,^{3,4} electrowetting,⁵ electrochemistry,⁶ thermocapillary pumping,⁷ and the use of magnetic fields.⁸

When the system is miniaturized to the submillimeter scale, the surface-to-volume ratio increases dramatically. As a consequence, surface properties of microchannels, especially wetting, have significant effects on the liquid behavior, which is embodied by the familiar phenomenon of liquids imbibing into glass capillaries. The capillary rise has been the basis of a simple and effective method to pump liquids into the microchannels.⁹ While water spontaneously flows into a pristine glass capillary, it does not penetrate a hydrophobically modified glass capillary unless pressure is applied. We have taken advantage of these surface effects to guide liquid flow inside surface-patterned microfluidic channels.¹⁰

Handique and co-workers^{11,12} reported on the fabrication of hydrophobic patches in microchannel networks to meter and pump discrete liquid drops by thermopneumatic pressure. The approach that they used is to modify the substrate surfaces with hydrophobic self-assembled monolayers (SAMs) in selected areas first and then align and bond substrates to form microchannel networks. A desired method would simultaneously pattern surface free energies on the top and bottom substrates in a preformed microchannel. We choose to work with microchannels made from glass slides and cover slips because their surface-wetting properties can be easily modified with SAMs and also because glass is transparent, allowing the use of an optical microscope to study liquid flow. It is well known that liquid flow is laminar in microchannels, which means multiple liquid streams can flow side

* To whom the correspondence should be addressed. E-mail: moore@scs.uiuc.edu.

[†] University of Illinois at Urbana–Champaign.

[‡] University of Wisconsin–Madison.

(1) Freemantle, M. *Chem. Eng. News* **1999**, 77 (8), 27–36.

(2) Harrison, D. J.; Fluri, K.; Seiler, K.; Fan, Z. H.; Effenhauser, C. S.; Manz, A. *Science* **1993**, 261, 895–897.

(3) Unger, M. A.; Chou, H. P.; Thorsen, T.; Scherer, A.; Quake, S. R. *Science* **2000**, 288, 113–116.

(4) Fahrenberg, J.; Bier, W.; Maas, D.; Menz, W.; Ruprecht, R.; Schomburg, W. K. *J. Micromech. Microeng.* **1995**, 5, 169–171.

(5) Prins, M. W. J.; Welters, W. J. J.; Weekamp, J. W. *Science* **2001**, 291, 277–280.

(6) Gallardo, B. S.; Gupta, V. K.; Eagerton, F. D.; Jong, L. I.; Craig, V. S.; Shah, R. R.; Abbott, N. L. *Science* **1999**, 283, 57–60.

(7) Burns, M. A.; Mastrangelo, C. H.; Sammarco, T. S.; Man, F. P.; Webster, J. R.; Johnson, B. N.; Foerster, B.; Jones, D.; Fields, Y.; Kaiser, A. R.; Burke, D. T. *Proc. Natl. Acad. Sci. U.S.A.* **1996**, 93, 5556–5561.

(8) Grant, K. M.; Hemmert, J. W.; White, H. S. *J. Am. Chem. Soc.* **2002**, 124, 462–467.

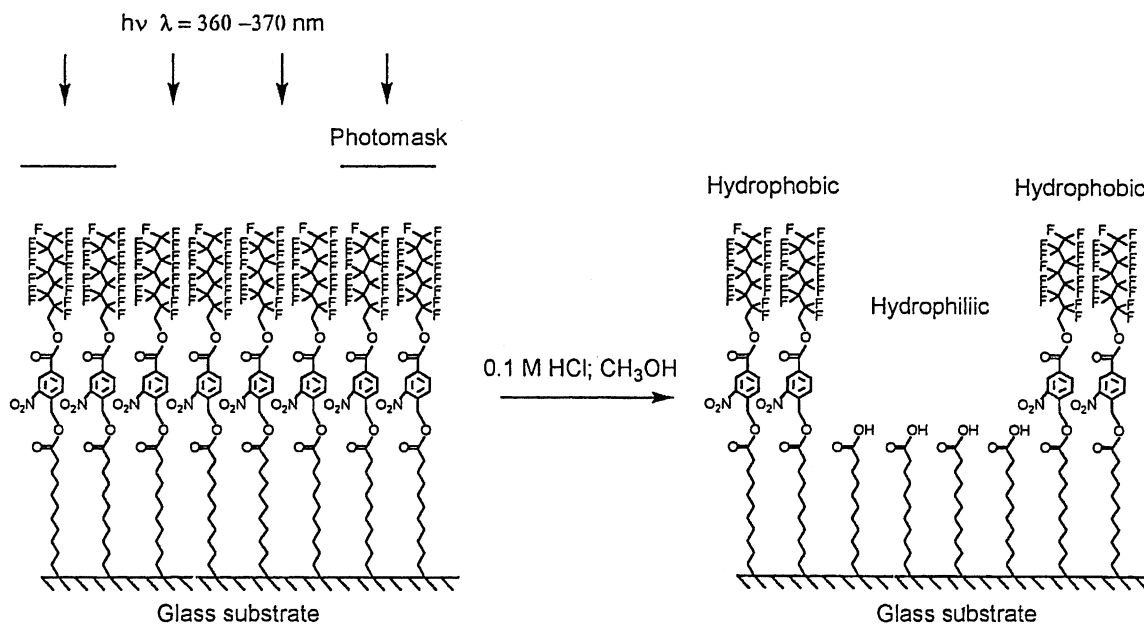
(9) Delamarque, E.; Bernard, A.; Schmid, H.; Michel, B.; Biebuyck, H. *Science* **1997**, 276, 779–781.

(10) Zhao, B.; Moore, J. S.; Beebe, D. J. *Science* **2001**, 291, 1023–1026.

(11) Handique, K.; Gogoi, B. P.; Burke, D. T.; Mastrangelo, C. H.; Burns, M. A. *Proc. SPIE–Int. Soc. Opt. Eng.* **1997**, 3224, 185–195.

(12) Handique, K.; Burke, D. T.; Mastrangelo, C. H.; Burns, M. A. *Anal. Chem.* **2001**, 73, 1831–1838.

Scheme 1. Photodeprotection of SAM of **2** upon UV Irradiation



by side without turbulence to maintain stationary interfaces.¹³ We have taken advantage of this flow behavior to fabricate surface patterns inside microchannels.¹⁰ Hexadecane and a solution of an organotrichlorosilane (e.g., octadecyltrichlorosilane (OTS)) in hexadecane were pumped into the preformed microchannels and maintained under laminar flow for a predetermined period of time until SAMs with full coverages formed. The areas where the silane solution passed were modified with SAMs and became hydrophobic, while other areas remained hydrophilic. Once the surface was patterned, aqueous solutions flow only along the hydrophilic pathway, provided the pressure is maintained below a critical value (thus we named the process surface-directed liquid flow). Because there are no physical walls on the sides of the liquid streams, the liquids are referred to as being confined by virtual walls. This method is simple, and patterning is complete in a short time, but it requires a preformed channel network and complex patterns cannot be easily generated. To overcome the limitations of the laminar flow fabrication method, we developed a photolithographic method to pattern surface free energies inside microchannels. With this method, all channel surfaces are first modified with photocleavable SAMs and then patterned by use of photomasks and UV light. The lithographic method is more flexible, allowing complex surface patterns to be fabricated.

In this paper, we detail our studies on surface-directed liquid flow from both theoretical and experimental approaches. The first part of this article is the synthesis, characterization, and properties of photocleavable SAMs. The second part consists of theoretical analyses and experimental investigations of the principles underlying the liquid flow inside surface-patterned channels. These principles include the maximum pressure that virtual walls can withstand, the critical width of the hydrophilic pathways that can support spontaneous flow, the smallest width of the liquid streams under an external pressure without entering the hydrophobic regions, the critical radius of curvature of a turn that can be

introduced into the hydrophilic pathway without liquid crossing the hydrophilic–hydrophobic boundary, and the minimal distance for two liquid streams to remain separated under the maximum pressure.

RESULTS AND DISCUSSION

Synthesis and Characterization of SAMs of Undecyl 4-(11-Trichlorosilyl-1-oxoundecyloxymethyl)-3-nitrobenzoate (1**) and 2,2,3,3,4,4,5,5,6,6,7,7,8,8,8-Pentadecafluoro-1-octyl 4-(11-Trichlorosilyl-1-oxoundecyloxymethyl)-3-nitrobenzoate (**2**).** An essential requirement in designing a photocleavable SAM for patterning surface free energies by ultraviolet (UV) photolithography is that the functional groups must be cleaved in long-wavelength UV light to avoid absorption by glass. *o*-Nitrobenzyl and related groups have been widely used as photocleavable protecting groups in organic synthesis and as photolabile linkages in solid-state synthesis of peptides.^{14–16} These groups are cleaved by UV light of wavelength longer than 320 nm, which is suitable for our purpose. Two photocleavable SAMs were designed by incorporation of *o*-nitrobenzyl groups, and their corresponding organotrichlorosilanes **1** and **2** were synthesized. As illustrated in Scheme 1, upon UV irradiation, the *o*-nitrobenzyl–oxygen bond is cleaved, and thus carboxylic acid groups are exposed to the air interface, making surfaces hydrophilic.

Synthesis of SAMs of **1 and **2**.** Organotrichlorosilanes **1** and **2** were synthesized through a three-step route as illustrated in Scheme 2. Esters **3** and **4** were prepared via a 1,3-dicyclohexylcarbodiimide (DCC) coupling reaction in yields of 65% and 64%, respectively. The synthesis of **5** and **6** followed the procedure reported by Shaw and co-workers.^{17,18} Hydrosilylation of alkenes **5** and **6** in the presence of catalytic hydrogen hexachloroplatinate-

(13) Kovacs, G. T. A. *Micromachined Transducer Sourcebook*; McGraw-Hill: Boston, 1998.

(14) Pillai, V. N. R. *Synthesis* **1980**, 1–26.

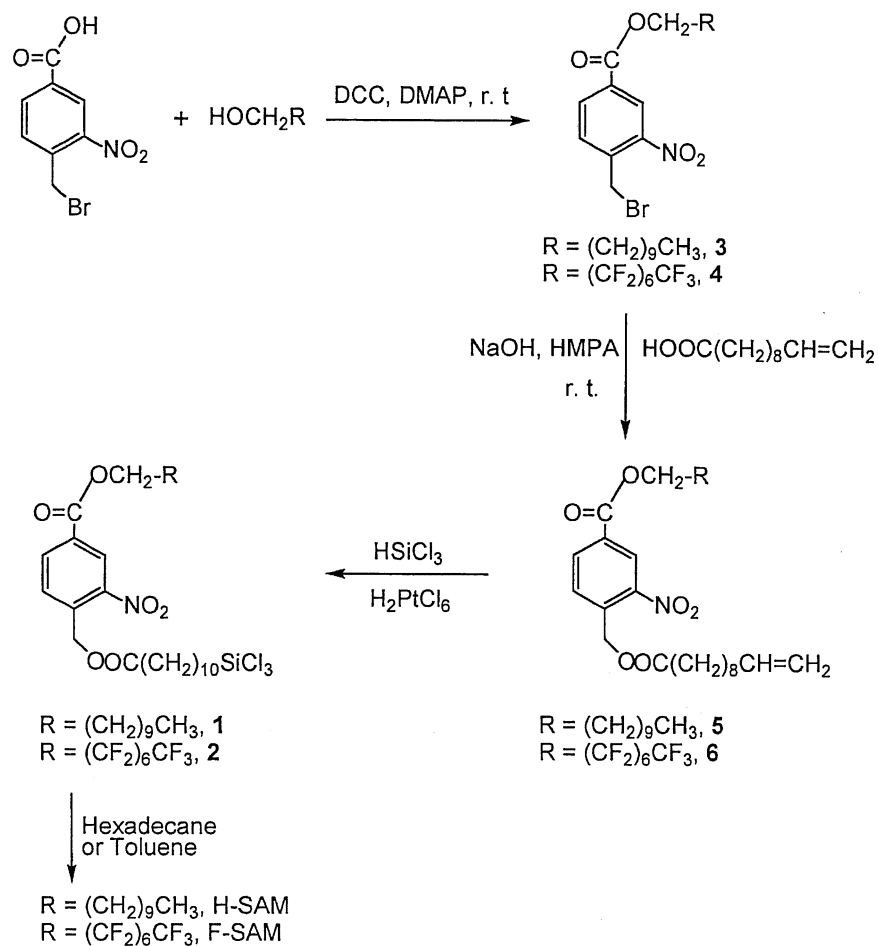
(15) Amit, B.; Zehavi, U.; Patchornik, A. *J. Org. Chem.* **1974**, *39*, 192–196.

(16) Rich, D. H.; Gurwara, S. K. *J. Am. Chem. Soc.* **1975**, *97*, 1575–1579.

(17) Shaw, J. E.; Kunerth, D. C. *J. Org. Chem.* **1974**, *39*, 1968–1970.

(18) Shaw, J. E.; Kunerth, D. C.; Sherry, J. J. *Tetrahedron Lett.* **1973**, *9*, 689–692.

Scheme 2. Synthesis of Photocleavable H-SAM and F-SAM



(IV) hydrate afforded the desired products, which were confirmed by ^1H and ^{13}C NMR. However, the base peaks in mass spectra obtained by field desorption are precursors (m/z 517.3 compared to m/z 517.2 of **5** and m/z 745.1 compared to m/z 745.2 of **6**) though the desired peaks m/z 652.2 and 882.0 appeared in low intensities. The trichlorosilyl groups were fragmented during ionization. The final products were used for SAM deposition without further purification.

High-quality SAMs of organotrchlorosilanes are not as easy to obtain compared to SAMs of alkanethiolates.^{19–24} Although extensive studies have been performed in the past two decades, the mechanism of SAM formation remains controversial. Many factors including organotrchlorosilane concentration, solvent, water content in the solvent, surface hydration of the substrate, humidity in the ambient environment, and temperature are known to influence the quality and coverage of SAMs.^{20,21} Two approaches were used to prepare photocleavable SAMs on cover glasses and inside microchannels. Microchannels were made according to a

method described in previous publications.^{25,26} In the first approach, “piranha”-treated cover glasses were immersed into a freshly prepared solution of **1** or **2** in dry hexadecane in a scintillation vial at room temperature. The silane solution was also injected into microchannels via a syringe. The optimal deposition time varied from 30 min to 4 h, depending on the ambient humidity, and was determined by measurement of advancing contact angles of H_2O on cover glasses. This approach is a conventional method to deposit SAMs on a “piranha”-treated silica substrate. In our experiments of formation of SAMs of **1** and **2** (in short, H-SAM and F-SAM, respectively), the deposition times varied from sample to sample even though the apparent reaction conditions were the same. Long deposition times lead to the precipitation of polymer formed in the bulk solution. To avoid this problem, a second method was used to prepare SAMs. A freshly prepared solution of **2** in toluene was allowed to age for a period until 1-min immersion of “piranha”-treated cover glasses resulted in a H_2O advancing contact angle of 118° for F-SAM.

Photodeprotection of H-SAM and F-SAM. Contact angle and X-ray photoelectron spectroscopy (XPS) were used to study the photodeprotection of H-SAM and F-SAM deposited on cover glasses. Figure 1 shows the relationships between UV irradiation time and the advancing contact angles (θ_a) of water and a NaOH

(19) Ulman, A. *Introduction to Ultrathin Organic Films: From Langmuir–Blodgett to Self-Assembly*; Academic Press: San Diego, CA, 1991.

(20) Ulman, A. *Chem. Rev.* **1996**, *96*, 1533–1554.

(21) Liu, Y.; Wolf, L. K.; Messmer, M. C. *Langmuir* **2001**, *17*, 4329–4335.

(22) Bunker, B. C.; Carpick, R. W.; Assink, R. A.; Thomas, M. L.; Hankins, M. G.; Voigt, J. A.; Sipola, D.; de Boer, M. P.; Gulley, G. L. *Langmuir* **2000**, *16*, 7742–7751.

(23) Le Grange, J. D.; Markham, J. L.; Kurkjian, C. R. *Langmuir* **1993**, *9*, 1749–1753.

(24) Tripp, C. P.; Hair, M. L. *Langmuir* **1995**, *11*, 149–155.

(25) Zhao, B.; Moore, J. S. *Langmuir* **2001**, *17*, 4758–4763.

(26) Beebe, D. J.; Moore, J. S.; Bauer, J. M.; Yu, Q.; Liu, R. H.; Devadoss, C.; Jo, B.-H. *Nature* **2000**, *404*, 588–590.

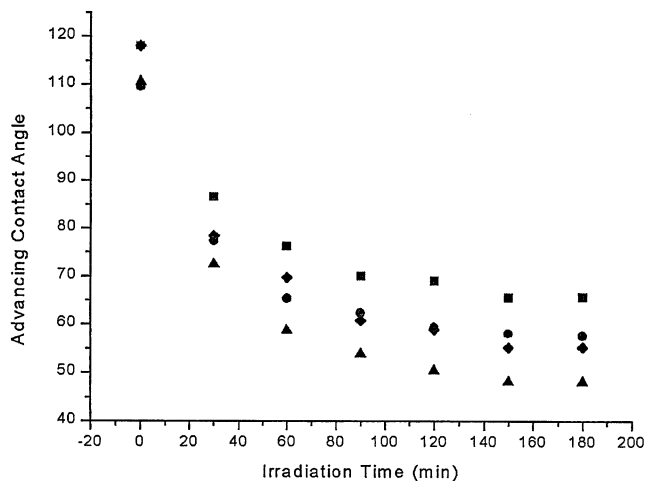


Figure 1. Effect of UV irradiation time on the surface-wetting properties of H-SAM and F-SAM: (●) Advancing contact angles of water on H-SAM; (■) advancing contact angles of water on F-SAM; (▲) advancing contact angles of pH = 11.8 NaOH solution on H-SAM; (◆) advancing contact angles of pH = 11.8 NaOH solution on F-SAM.

solution (pH = 11.8) on H-SAM and F-SAM. The θ_a of both H₂O and the NaOH solution decrease significantly during the early irradiation period and level off after 90 min. The lowest values of H₂O θ_a on irradiated H-SAM and F-SAM are 58° and 66°, respectively. The values of θ_a of the NaOH solution on both irradiated H-SAM and F-SAM are ~10° lower than those of water. This is consistent with carboxylic acid-terminated surfaces as a basic probe liquid ionizes the immobilized carboxylic acid groups making the surface more wettable.²⁷ The values of θ_a of both water and the NaOH solution on F-SAM are ~8° higher than those on H-SAM after being irradiated by UV light for 3 h. XPS studies indicate that the photochemical reaction is not complete or some side reactions might occur (vide infra). A trace amount of fluorine atoms on the surface can increase the observed advancing values relative to alkyl chains, assuming the extent of photochemical reactions is the same for both H-SAM and F-SAM. The values of water θ_a on carboxylic acid-terminated monolayers achieved here are much higher than those of water on carboxylic acid- or hydroxyl-terminated SAMs of alkanethiolates (both are 0°)¹⁹ but close to those of water on hydroxyl- and phenol-terminated monolayers (63° and 58°, respectively) obtained via surface reactions from the corresponding SAMs of trichlorosilanes.^{28,29} Besides the incomplete photodeprotection that will be discussed later, there is another possible factor responsible for the high values of water θ_a . The structures of SAMs of organotrichlorosilanes are known to be less ordered than those from organothiols. Polar functional groups on the surface are susceptible to surface reorganization. More methylene groups exposed to the air interface will make θ_a higher. The advancing contact angles of water on hydroxyl-terminated monolayers have been reported to be heavily dependent on how the samples are treated.^{19,30}

Photodeprotection of H- and F-SAM can be much faster if a higher intensity UV light source is used. For instance, a similar

trend of θ_a decrease with irradiation time was observed but ~60× faster when Novacure (EFOS, model N2001-A1) with a 365-nm filter was used as the UV light source with a preset intensity of 5600 mW/cm² and a distance between the lens and the channels of 20 mm. The ability to control the surface wettability by UV irradiation time gives us a means to continuously vary surface-wetting properties. By combining this advantage and the principles of surface-directed liquid flow, we have fabricated a series of pressure-sensitive gates to regulate liquid flow.³¹

XPS Characterization. XPS is especially suitable for the study of photodeprotection of H-SAM and F-SAM as *o*-nitrobenzyl groups are cleaved after UV irradiation. In both spectra of H- and F-SAMs before UV irradiation shown in Figures 2a and 3a, nitrogen peaks N_{1s} are found located at ~405 eV, which are attributed to the nitrogen in *o*-nitrobenzyl groups.³² Curves b in Figures 2 and 3 were recorded from a H-SAM and a F-SAM both irradiated by UV light for 2.5 h. The nitrogen peaks at ~405 eV were not detectable. Although the fluorine peak shrank drastically after irradiation in F-SAM, it did not disappear completely, which implies that the photoreaction is not complete.

Considering that the advancing contact angle of water changes little with increasing UV irradiation time, some side reactions might occur as discussed in the literature.¹⁴ A new nitrogen peak was found at ~400 eV, which we attributed to the contaminant from air. It is known that the rate of contamination of acidic or basic surfaces is rapid in air.³³

Contact Angle Titration of Carboxylic Acid-Terminated Monolayers. Contact angle titration is a method to study the wettability of ionizable surfaces as a function of pH of the probe liquids.³³ We followed a procedure similar to those described in the literature^{27,28,34} to perform contact angle titration of carboxylic acid-terminated monolayers obtained by photodeprotection of H- and F-SAMs. A series of aqueous buffered solutions prepared by properly combining NaH₂PO₄, Na₂HPO₄, HCl solution, and NaOH were used. The results are summarized in Figure 4. For both surfaces, θ_a is independent of pH in the range of 2–5 and starts to decrease at a pH of 5.5. Little change is observed at pH above 9.0. Clearly, the surface is more wettable at high pH values as probe liquids of high pH values ionize carboxylic acid groups. The changes of θ_a are reversible. Consider Young's equation $\gamma_{lv} \cos \theta = \gamma_{sv} - \gamma_{sl}$, where γ_{lv} , γ_{sv} , and γ_{sl} are surface free energies of liquid–gas, solid–gas, and solid–liquid interfaces, respectively, and θ is the contact angle. Assuming that γ_{lv} and γ_{sv} vary little with respect to pH, the changes of γ_{sl} are responsible for the decrease of contact angle at high pH values. If we assume that the carboxylic acid groups are protonated at low pH (<5) and completely ionized at high pH, we can infer the acidity of surface-bound carboxylic acid $pK_{1/2}$ as described by Lee and co-workers.³³ $pK_{1/2}$ is analogous to pK_a in solution and is defined as the value of the pH of the solution at which the functional groups at the interface are half-ionized. Sigmoidal fitting indicates that the transition ($pK_{1/2}$) occurs at pH = 6.90 and pH = 7.05 for carboxylic acid-terminated monolayers obtained from H- and F-SAMs,

(31) Zhao, B.; Moore, J. S.; Beebe, D. J. Manuscript to be submitted.

(32) Briggs, D. *Surface Analysis of Polymers by XPS and Static SIMS*; Cambridge University Press: Cambridge, U.K., 1998.

(33) Lee, T. R.; Carey, R. I.; Biebuyck, H. A.; Whitesides, G. M. *Langmuir* **1994**, *10*, 741–749.

(34) Holmes-Farley, S. R.; Reamey, R. H.; McCarthy, T. J.; Deutch, J.; Whitesides, G. M. *Langmuir* **1985**, *1*, 725–740.

(27) Bain, C. D.; Whitesides, G. M. *Langmuir* **1989**, *5*, 1370–1378.

(28) Zhao, B.; Mulkey, D.; Brittain, W. J.; Chen, Z.; Foster, M. D. *Langmuir* **1999**, *15*, 6856–6861.

(29) Heid, S.; Effenberger, F.; Bierbaum, K.; Grunze, M. *Langmuir* **1996**, *12*, 2118–2120.

(30) Tillman, N.; Ulman, A.; Penner, T. L. *Langmuir* **1989**, *5*, 101–111.

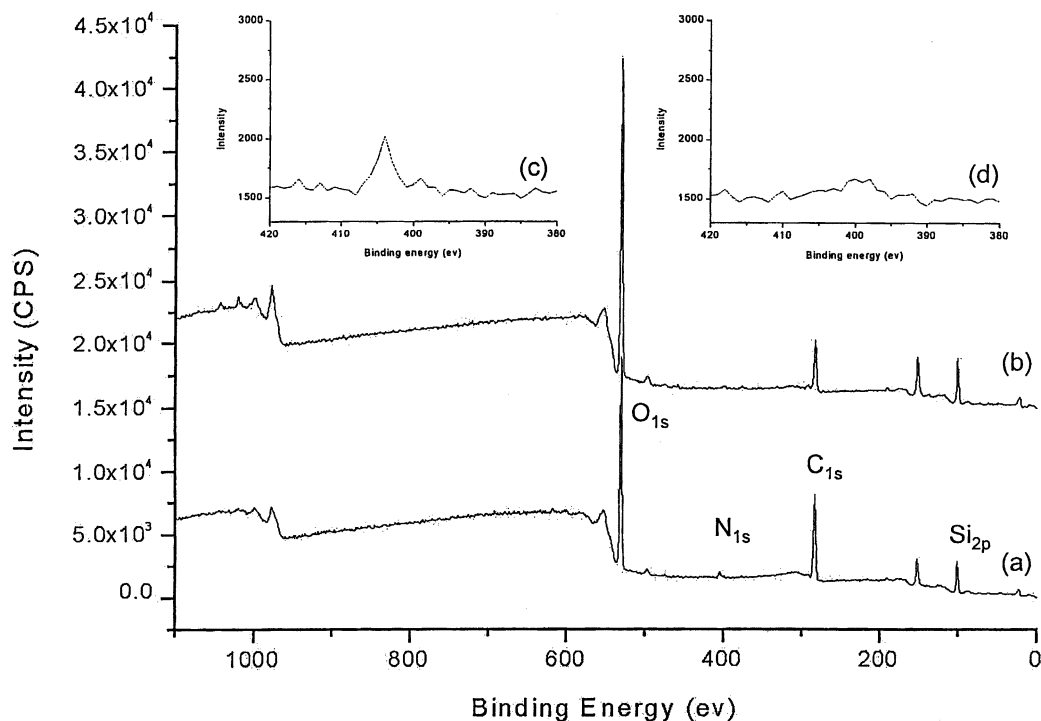


Figure 2. XPS spectra of H-SAM deposited on "piranha"-treated cover glasses (a) before and (b) after UV irradiation. (c) N_{1s} area in curve a. (d) N_{1s} area in curve b.

respectively. Compared to the pK_a of formic acid (3.74) and acetic acid (4.76) in aqueous solutions, the values of $pK_{1/2}$ derived here are higher by about 2–3 pH units. These results are consistent with that of carboxylic acid on a polyethylene surface obtained by chromic acid oxidation.³⁴ Holmes-Farley and co-workers attributed the shift of $pK_{1/2}$ relative to the solution pK_a to the difficulties in the formation of carboxylate ions at the solid–liquid interface due to the low dielectric constant at the interface or charge–charge interaction.³⁴

The contact angle titration studies thus provide further evidence that carboxylic acid-terminated monolayers were obtained by photodeprotection of H- and F-SAMs. We have taken advantage of the changes of advancing contact angles with respect to pH to fabricate pH-sensitive gates to regulate liquid flow inside surface-patterned channels.³¹

Principles of Surface-Directed Liquid Flow inside Microchannels. In this section, we discuss the principles underlying the liquid flow in surface-patterned microfluidic channels using both analytical and experimental approaches. A variety of hydrophilic–hydrophobic surface patterns have been fabricated by use of either the laminar flow or photolithography fabrication method.

Principle 1: Critical Pressure That Virtual Walls Can Withstand. Aqueous solutions flow only along the hydrophilic pathways in surface-patterned microchannels when the pressure is maintained below a critical value. The gas–liquid interface is pinned precisely at the boundary between the hydrophilic and hydrophobic regions, and the liquid will curve outward if a pressure is applied (Figure 5). Liquid streams will rupture the virtual walls and flow into the hydrophobic regions if the angle of curvature of the liquid at the hydrophilic–hydrophobic boundary (θ_b) equals the advancing contact angle of the liquid on the nonpolar surface (θ_n). When a liquid surface is curved, there is a pressure drop across the interface due to the liquid surface

tension. This is described by the Young-Laplace equation, $\Delta P = \gamma(1/R_1 + 1/R_2)$, where ΔP is the pressure difference, γ is the liquid surface tension, and R_1 and R_2 are the radii of curvature in directions vertical and parallel to the liquid stream.³⁵ For a straight stream, the equation is simplified to $\Delta P = \gamma/R_1$. The parameter R_1 is related to the channel depth h and θ_b through the equation, $R_1 = h/[2 \sin(\theta_b - 90^\circ)]$. When $\theta_b = \theta_n$, the maximum pressure that virtual walls can sustain in a straight stream, is realized, $P_{\max} = \Delta P = (2\gamma/h) \sin(\theta_n - 90^\circ)$. Obviously, θ_n must be greater than 90° for liquids to be confined to the hydrophilic regions by virtual walls. Experimentally, we observed that hexadecane was not confined to the hydrophilic pathways generated from photocleavable F-SAM, which is consistent with the fact that the θ_n of HD on F-SAM is 74° , i.e., smaller than 90° .³⁶ The channel depth is $\sim 180 \mu\text{m}$, and the values of θ_n of water on SAMs of OTS and heptadecafluoro-1,1,2,2-tetrahydrodecyltrichlorosilane (HFTS) are 112° and 118° , respectively. Calculations show that the P_{\max} for OTS and HFTS are 300 ($30.6 \text{ mm H}_2\text{O}$) and 376 N/m^2 ($38.4 \text{ mm H}_2\text{O}$), respectively. We used surface-patterned channels fabricated by multistream laminar flow in combination with SAMs of either OTS or HFTS to measure the maximum pressures. Experimental results are 31-mm water for OTS-patterned channels and 37-mm water for HFTS-patterned channels, in good agreement with our analytical predictions.¹⁰

Principle 2: Critical Width of the Hydrophilic Pathways That Can Support Spontaneous Liquid Flows. Figure 6a illustrates the tip of an advancing liquid stream in a surface-patterned channel. The advancing contact angle of water on virtual walls can be viewed as 180° since small water drops assume a

(35) Adamson, A. W. *Physical Chemistry of Surfaces*, 5th ed.; Wiley: New York, 1990.

(36) Zhao, B. Viernes, N. O. L.; Moore, J. S.; Beebe, D. J. *J. Am. Chem. Soc.* **2002**, *124*, 5284–5285.

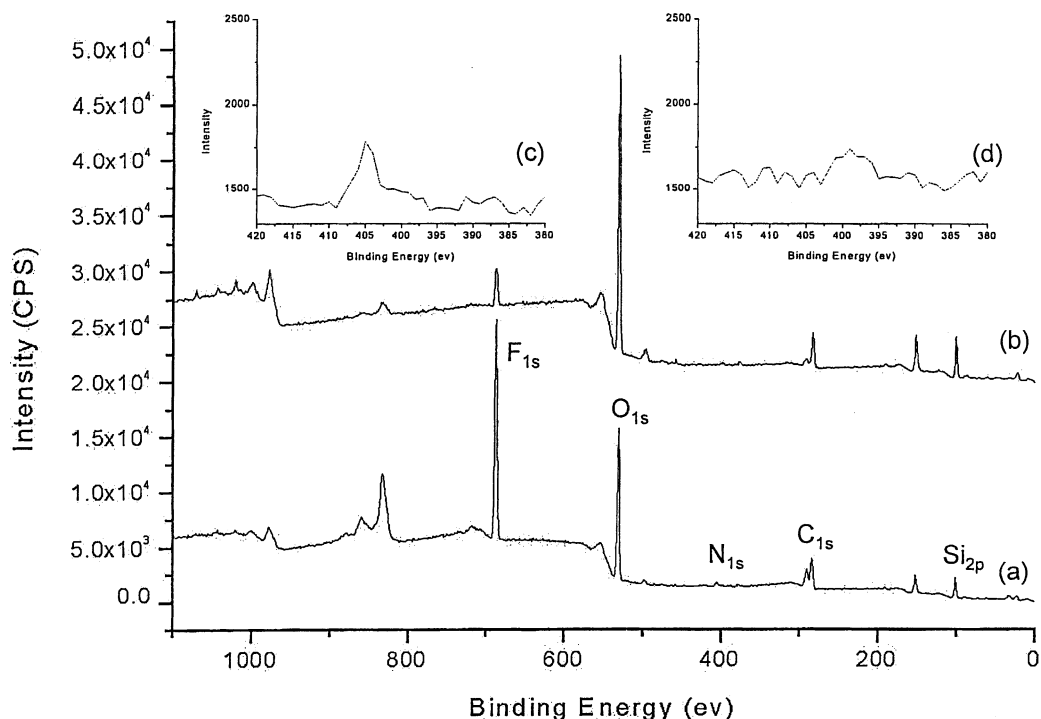


Figure 3. XPS spectra of F-SAM deposited on "piranha"-treated cover glasses (a) before and (b) after UV irradiation. (c) N_{1s} area in curve a. (d) N_{1s} area in curve b.

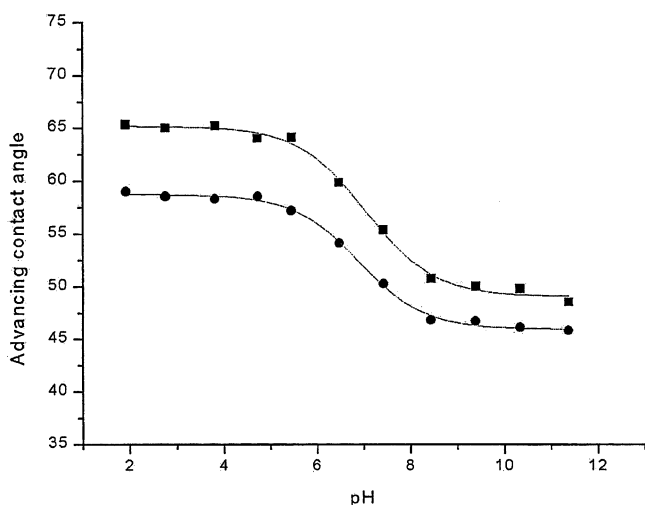


Figure 4. Advancing contact angles of aqueous buffered solutions on carboxylic acid-terminated monolayers obtained from H-SAM and F-SAM by UV irradiation. (●) Monolayer obtained from H-SAM; (■) monolayer obtained from F-SAM. The curves were from sigmoidal fitting.

round shape in air. The aqueous solution in the hydrophilic pathway is actually confined by top and bottom hydrophilic surfaces separated by distance h and two hydrophobic virtual walls spaced by width w . The capillary force generated from the hydrophilic surfaces drives liquid forward as in a pristine glass capillary, producing a side-view profile shown in Figure 6b with a negative R_1 , whereas the retraction force generated from the hydrophobic virtual walls drags water backward, producing a top-view profile shown in Figure 6c with a positive R_2 . These two forces counteract each other and determine the critical geometry of the pathway. If $|R_2| > |R_1|$, $\Delta P < 0$ and water spontaneously wets the hydrophilic pathway. If $|R_2| < |R_1|$, $\Delta P > 0$ and water

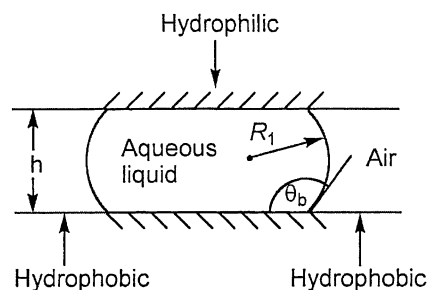


Figure 5. Angle of curvature θ_b of a liquid confined to the hydrophilic region inside a microchannel.

does not spontaneously flow through the hydrophilic region. The critical condition occurs when $|R_2|$ is equal to $|R_1|$ (i.e., $\Delta P = \gamma \cdot (1/R_1 + 1/R_2) = 0$), which is satisfied when $w = h/(\cos \theta_p)$. If the hydrophilic region is completely wetted by aqueous liquids ($\theta_p = 0^\circ$), the critical width of the liquid stream is equal to the channel depth. A higher contact angle in the hydrophilic pathway requires a larger width for flow to take place spontaneously.

We used a wedge-shaped photomask shown in the upper left corner of Figure 6d to fabricate a surface pattern inside a channel to verify the above analytical expression. The channel surface was deposited with F-SAM. The UV irradiation time was 2 h. The introductory pathway was also irradiated so that liquids flow spontaneously through the entrance. Figure 6d and e shows the optical micrographs of where water and the NaOH solution (pH = 11.8) reached in the wedge-shaped hydrophilic pattern under spontaneous flow conditions. The images were taken when liquids did not move forward any more (it took a few minutes after liquids were introduced). The tips of both liquid streams exhibit round shapes as expected in the theoretical analysis. We used circles to fit the tips, and the diameters of the fitting circles are 442 and 359 μm for water and the NaOH solution, respectively. By use of

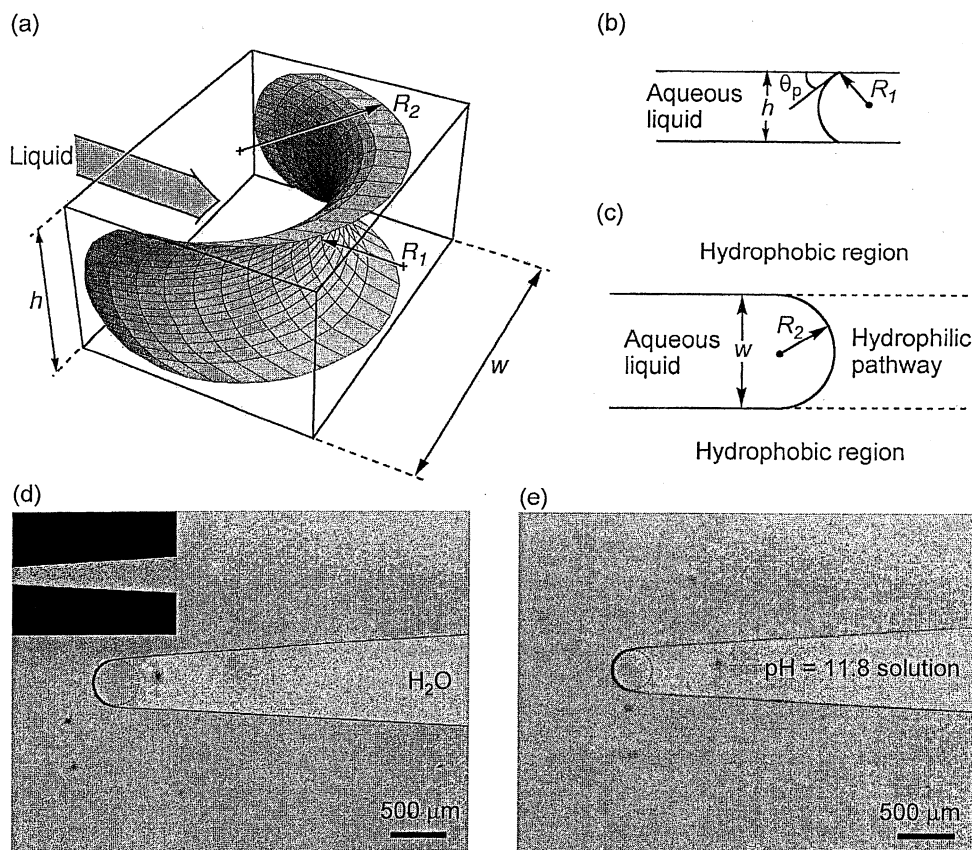


Figure 6. (a) Schematic illustration of the tip of a liquid advancing along a hydrophilic pathway. (b) Side-view profile and (c) top-view profile of the tip of the advancing liquid stream confined to the hydrophilic pathway. Optical micrographs of where water (d) and the pH = 11.8 NaOH solution (e) stop in a wedge-shaped pathway under spontaneous flow conditions. The dash circles are used to fit the tips of liquid streams for determination of the critical widths. The surface pattern was fabricated by use of the photomask shown in the upper left corner of image d.

the critical width equation derived above, the calculated advancing contact angles of water and the NaOH solution on the hydrophilic region are 66° and 60° , which are in good agreement with the results measured on a F-SAM-coated cover glass irradiated by UV light for the same length of time (69° and 59° for water and the NaOH solution (pH = 11.8) in Figure 2, respectively).

Principle 3: Smallest Width of Liquid Streams under External Pressures. If a pressure is applied to a liquid stream confined to the wedge-shaped hydrophilic region, it will flow into a narrower portion of the hydrophilic pathway. As discussed in principle 2, the pressure drop across the liquid interface in the tip of a liquid stream is described by Young–Laplace equation $\Delta P = \gamma (1/R_1 + 1/R_2)$, where R_1 and R_2 are defined as the radii of curvature in directions vertical and parallel to liquid stream. The critical condition under an external pressure occurs when the sum of the external pressure and capillary force γ/R_1 generated from the hydrophilic physical walls equals the retraction force generated from hydrophobic virtual wall γ/R_2 ; that is, $P + \gamma/R_1 = \gamma/R_2$. The pressure, P , can be expressed in terms of the water height H . Therefore, $1/w = (\rho g/2\gamma)H + \cos \theta_p/h = (\rho g/2\gamma)H + 1/w_0$, where ρ is the liquid density and w_0 is the critical width of liquid streams under spontaneous flow conditions.

Experimentally, we used a wedge-shaped hydrophilic surface pattern to investigate the smallest width of liquid streams under external pressures. The images were taken when the liquid was no longer moving under a certain pressure. The tip was fitted with a circle, and the diameter was measured. Figure 7 shows

the calculated values and experimental results of the smallest width of a liquid stream under external pressures. Although the trend of the decrease in the smallest width with increasing external pressure is qualitatively consistent with the theoretical curve, there is a discrepancy between the theoretical predictions and experimental data. This discrepancy may come from some factors that have not been taken into account. For example, the advancing contact angle of an aqueous liquid on the hydrophilic region surrounded by the hydrophobic surface under a pressure may not be the same as obtained in the contact angle measurement. More investigations regarding this issue are needed and are underway.

Principle 4: Critical Radius of Curvature of Turns That Liquids Can Make under Spontaneous Flow Conditions. Liquids do not have their own shapes but assume the shapes of their containers. In surface-patterned channels, water is confined to the hydrophilic region by only two physical walls, raising questions such as how well the liquid shape can be controlled. If a turn is introduced in the hydrophilic pathway as illustrated in Figure 8a, the radius of curvature in the direction parallel to the liquid stream, R_2 , is finite. For the outer virtual wall, R_2 is positive and thus the maximum pressure that the outer virtual wall can withstand increases. For the inner virtual wall, R_2 is negative, and consequently, the maximum pressure decreases. Thus, there is a limit on the sharpness of the turns that can be introduced without the liquid crossing the boundary. The critical condition occurs at $\Delta P = 0$, that is, $R_1 = R_2$. The smallest R_1 is realized

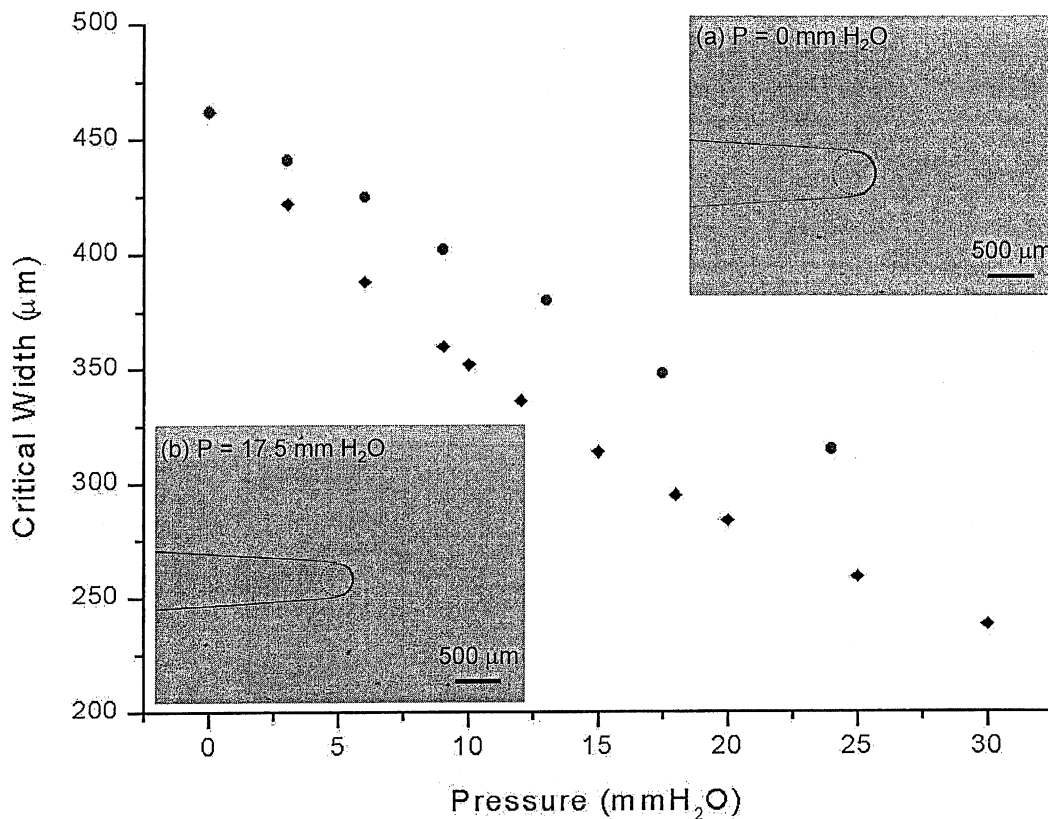


Figure 7. Relationship between the smallest width of liquid stream and external pressures. (●) Experimental results; (◆) calculated values. Optical micrographs of where water stops at a pressure of (a) 0 and (b) 17.5 mm H₂O in a wedge-shaped hydrophilic surface pattern. The dash circles are used to fit the tips of liquid streams for determination of the critical widths.

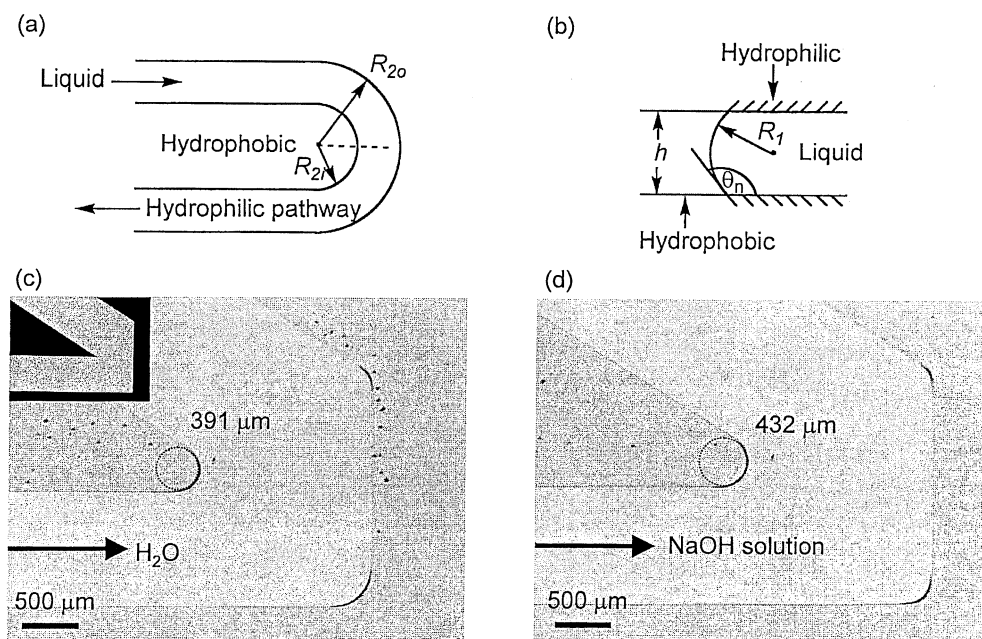


Figure 8. (a) Top-view profile of a turn introduced into a hydrophilic pathway. (b) Side-view profile along the dash line in the top-view profile. Optical micrographs of (c) water and (d) pH = 11.8 NaOH solution streams making turns. The dash circles are used to fit the inner edges for determination of the critical radius of curvature of turns. The surface pattern was fabricated by use of the photomask shown in the upper left corner of image c in a reduced scale. The images were taken when liquid edges were no longer moving.

when $\theta_b = \theta_n$. Therefore the critical radius of curvature is $|R_{2ic}| = |R_1| = h/[2 \sin(\theta_n - 90^\circ)]$. For $h = 180 \mu\text{m}$ as used here, calculation shows that the critical radii of curvature of the turns are $240 \mu\text{m}$ in H-SAM-modified channel and $192 \mu\text{m}$ in F-SAM-modified channels.

We used a photomask shown in Figure 8c to fabricate a surface pattern inside a F-SAM-coated channel. The introductory pathway was also irradiated by UV light so that aqueous solutions can advance into the hydrophilic pathway spontaneously. Figure 8c and d shows the images of water and the NaOH solution (pH =

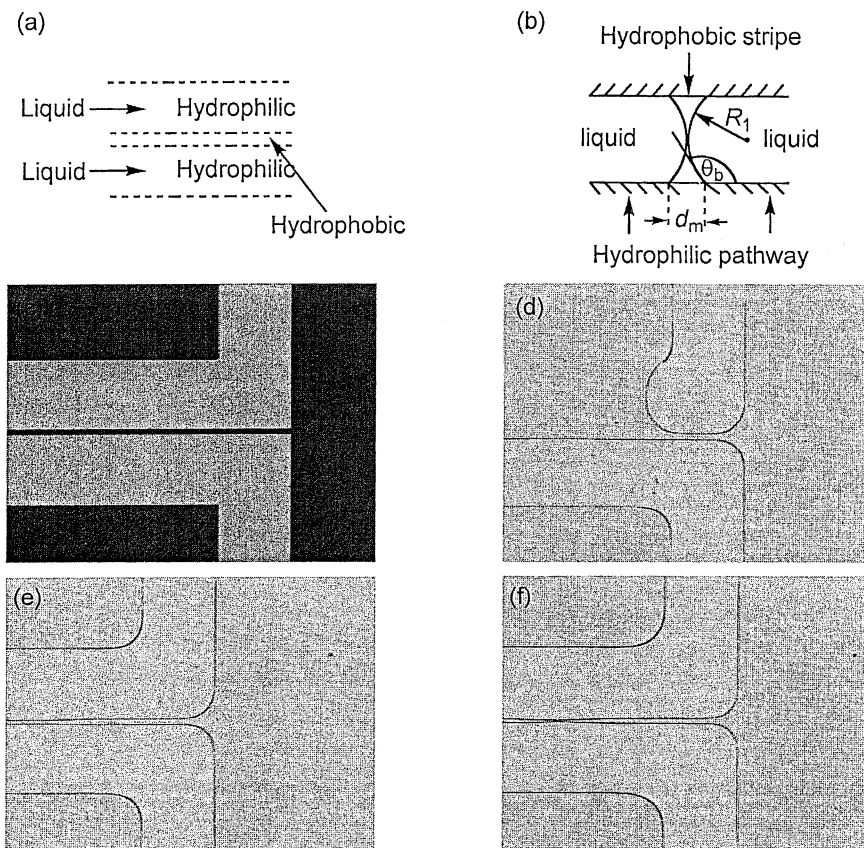


Figure 9. (a) Top-view profile of two liquid streams separated by a hydrophobic stripe with a width of d_m . (b) Side-view profile of two liquid streams remaining separated under the maximum pressure. (c) The photomask used in the fabrication of two hydrophilic pathways separated by a 50- μm hydrophobic stripe. Optical micrographs of water streams (d) under spontaneous flow conditions, pressures of (e) 5- and (f) 12-mm water.

11.8) flowing into the hydrophilic pathways spontaneously. The images were recorded when the edges were no longer moving (~ 10 min after the solution was introduced). As expected, the inner edges smoothed out and exhibited rounded shapes. Moreover, they are thicker than the straight edges, which indirectly indicates the liquid–gas interface curves outward. We used circles to fit the inner edges and measured the diameters of the circles. The results were 391 and 432 μm for water and the basic solution streams, respectively, close to the calculated values (384 μm). The advancing contact angles of water and the basic solution were the same on the F-SAM surface. The differences between the radii of curvature of turns made by water and the NaOH solution are attributed to kinetic factors. It was observed that the flow rate of the basic solution was higher than water on the same hydrophilic pathways due to its lower advancing contact angle. This kinetic factor causes the NaOH solution to flow into the hydrophobic region more than under an equilibrium condition. Obviously, liquids cannot make a very sharp turn because of the liquid surface tension effect. However, if we decrease the channel height and increase the advancing contact angle (e.g., through controlling the surface roughness³⁷), it would be possible to better control the liquid shape.

Principle 5. Minimum Distance for Two Liquid Streams To Remain Separated under the Maximum Pressure. A high density of microchannels or liquid streams in a microfluidic chip

is desired for fabricating compact microfluidic devices and for performing fast manipulations. In surface-directed liquid flow, two liquid streams can be extremely close to each other while remaining separated under a condition of no pressure if the boundary between the hydrophilic and hydrophobic regions is ideally sharp. An external pressure applied to the liquid streams will cause the gas–liquid interface to bulge out and flow into the hydrophobic region if the angle of curvature θ_b at the hydrophilic–hydrophobic boundary equals the θ_n of the liquid on the hydrophobic region. Figure 9a and b shows the top-view and side-view profiles of two liquid streams flowing parallel to each other separated by a hydrophobic stripe of width d under the maximum pressure. The minimum distance for two streams to remain separated under the maximum pressure can be calculated on the assumptions that the boundary between the hydrophilic and hydrophobic regions are infinitely sharp and two gas–liquid interfaces come in contact at the critical condition $\theta_b = \theta_n$ as shown in Figure 9b. Thus, the minimum distance is $d_m = 2[R_1 - R_1 \cos(\theta_n - 90^\circ)] = h[1 - \cos(\theta_n - 90^\circ)]/\sin(\theta_n - 90^\circ)$. It is apparent that the minimum distance is determined by two parameters, h and θ_n . Calculations indicate that the values of d_m for water in patterned H-SAM- and F-SAM-coated channels are 35 and 45 μm , respectively for h of ~ 180 μm .

We patterned a surface consisting of two hydrophilic stripes separated by a 50- μm hydrophobic stripe by use of the photomask shown in Figure 9c inside a F-SAM-coated channel. The UV

(37) Johnson, R. E.; Dettre, R. H. *Adv. Chem. Ser.* **1964**, *43*, 112.

irradiation time was 130 min. Water flowed into the hydrophilic regions spontaneously (Figure 9d). Figure 9e and f shows the images of water streams under pressures of 5- and 12-mm water, respectively. Although we could not image the side-view profile, it is clear that the boundaries of the liquid streams became thicker and approached one another with increasing the pressure, which indirectly indicated that the gas–liquid interface bulged out. Owing to the intrinsic resolution limit of transparency film photomasks, the boundary between the hydrophilic and hydrophobic regions is more or less distorted on the scale of $\sim 10 \mu\text{m}$.³⁸ Since the channel depth is $\sim 180 \mu\text{m}$, more than 3 times larger than the hydrophobic gap, the fidelity between the photomask and surface patterns on top and bottom substrates is also dependent on whether the UV light is perfectly collimated. We speculate that these two factors are responsible for the defect appearing in images c and d. Nevertheless, we have shown that the resolution of surface patterns fabricated by use of our current photolithography method can reach $\sim 20 \mu\text{m}$.

Conclusions. SAMs were used in combination with either multistream laminar flow or photolithography to pattern surface free energies inside channels to direct liquid flow. Aqueous solutions flow only along the hydrophilic pathways provided the pressure is maintained below a critical value. For use in photolithography, two photocleavable SAMs of organotrichlorosilanes were designed and successfully prepared. Photodeprotections were investigated by contact angle, XPS, and contact angle titration. XPS study indicated that the photodeprotection reaction was close to complete after UV irradiation for 2.5 h. A small fluorine peak existing in the XPS of the UV-irradiated F-SAM and little change in contact angle with a longer irradiation time implied that some side reactions occur. Contact angle titration further proved that carboxylic acid-terminated monolayers were obtained. The acidities, $\text{p}K_{1/2}$, of surface-bound carboxylic acid obtained from H- and F-SAM were derived from the titration curves and were found to be 2–3 pH units higher than the solution $\text{p}K_a$. Although these two SAMs perform similarly, their differences in initial values of θ_a and final values of θ_a after UV irradiation give us a flexibility in controlling surface wettabilities. The principles governing the liquid flow in the surface-patterned channels were investigated analytically and experimentally. The analytical equations were derived based on the Young–Laplace equation. The maximum

pressure that virtual walls can withstand in a straight stream is $P_{\text{max}} = (2\gamma/h) \sin(\theta_n - 90^\circ)$. The critical width of the hydrophilic pathways that can support spontaneous liquid flow is $w = h/(\cos\theta_p)$. The smallest width that allows liquid stream to flow in under an external pressure is $1/w = (\rho g/2\gamma)H + \cos\theta_p/h$. The critical radius of curvature of turns that can be introduced in the hydrophilic pathways without liquid flowing into the hydrophobic regions is $h/[2 \sin(\theta_n - 90^\circ)]$. The minimum distance for two liquid streams to remain separated under maximum pressure is $d_m = h[1 - \cos(\theta_n - 90^\circ)]/\sin(\theta_n - 90^\circ)$. A series of surface patterns were designed and fabricated inside channels to verify these equations. Experimental results are in good qualitative agreement and generally good quantitative agreement with the analytical values. Because surface-directed liquid flow requires only two physical walls, a large gas–liquid interface is created, which enables gas–liquid reactions to be performed in a more controlled way.¹⁰ We believe that the principles underlying surface-directed liquid flow and the methods that we developed to generate surface patterns will find a broad range of applications in microfluidic systems including chemical and biological analysis and microreactors, especially where gaseous fluids are involved.

ACKNOWLEDGMENT

This work was financially supported by grants from the Defense Advanced Research Projects Agency-MTO F30602-00-1-0570 and NSF DMR 01-06608. XPS measurements were carried out at the Materials Research Laboratory center for Microanalysis of Materials, which is supported by the Department of Energy through Grant DE FG0296R45439. Funding for the Kratos Axis ULTRA XPS system was provided by the National Science Foundation through Grant NSFDMR 99-77482 and the State of Illinois. We acknowledge Dr. Rick Haasch for his help in XPS measurement.

SUPPORTING INFORMATION AVAILABLE

Experimental procedure for the preparation of **1** and **2** and their characterization data. Experimental procedure for H-SAM and F-SAM formation and photodeprotection. This material is available free of charge via the Internet at <http://pubs.acs.org>.

Received for review April 25, 2002. Accepted May 22, 2002.

AC020269W

(38) Love, J. C.; Wolfe, D. B.; Jacobs, H. O.; Whitesides, G. M. *Langmuir* **2001**, *17*, 6005–6012.